Implementing a plant hydraulics parameterization in the Canadian Land Surface Scheme Including biogeochemical Cycles (CLASSIC) v.1.4

Muhammad Umair[1], Joe R. Melton[2], Alexandre Roy[3], Cleiton B. Eller[4], Jennifer Baltzer[5], Bram Hadiwijaya[1,6], Bo Qu[1], Nia Perron[1,7], Oliver Sonnentag[1]

[1]Département de géographie, Université de Montréal, Montréal, QC, H2V 2B8, Canada.
[2]Climate Research Division, Environment and Climate Change Canada, Victoria, B.C., V8W 3V6, Canada.
[3]Département des Sciences de l'Environnement, Université du Québec à Trois-Rivières (UQTR), Trois-Rivières, Québec, G9A 5H7, Canada.
[4]Department of Biology, Federal University of Ceará, Fortaleza, Brazil.
[5]Department of Biology, Wilfrid Laurier University, Waterloo, ON, N2L 3C5, Canada.
[6]Department of Sustainability Research, SMART Research Institute, Riau, 28686, Indonesia.
[7]Institut des sciences de la forêt tempérée (ISFORT), Université du Québec en Outaouais (UQO), 58 rue principale, Ripon, QC J0V 1V0, Canada

Key Points:

- A plant hydraulics parameterization was included in the Canadian Land Surface Scheme Including biogeochemical Cycles
- Evaluated at eight boreal forest flux tower sites, the new parameterization improved overall simulation of gross primary production
- During drought periods, in particular, the new plant hydraulics parameterization outperforms the original soil moisture stress-based approach

Corresponding author: Oliver Sonnentag, Muhammad Umair, `oliver.sonnentag@umontreal.ca`, `muhammad.umair.1@umontreal.ca`

Abstract

Drought conditions caused by soil moisture stress and/or high vapour pressure deficit pose a challenge to many terrestrial ecosystem models (TEMs). The Canadian LAnd Surface Scheme Including biogeochemical Cycles (CLASSIC) employs an empirical approach to link soil moisture stress with stomatal conductance. Such soil moisture-based empirical approaches typically perform poorly during drought. Here, we implemented an explicit plant hydraulics parameterization, i.e., Stomatal Optimization based on Xylem hydraulics (SOX), in CLASSIC, thereby connecting the soil-plant-atmosphere continuum through plant hydraulic traits. Performance of the resulting CLASSIC$_{SOX}$ was evaluated against carbon and water fluxes measured with eddy covariance at eight boreal forest flux tower sites in North America. Compared to CLASSIC, CLASSIC$_{SOX}$ better simulated gross primary productivity (GPP) across all sites, i.e., coefficient of determination (R^2) increased (0.51 to 0.59), root mean square error (RMSE) and bias decreased (1.85 to 1.54 g C m^{-2} d^{-1}) and (-0.99 to -0.58 g C m^{-2} d^{-1}), respectively. Under drought conditions, identified using the Palmer drought severity index, GPP simulated with CLASSIC$_{SOX}$ improved compared to CLASSIC, i.e., R^2 increased (0.51 to 0.60), and RMSE and bias decreased (1.79 to 1.46 g C m^{-2} d^{-1}) and (-0.97 to -0.53 g C m^{-2} d^{-1}), respectively. In contrast, CLASSIC$_{SOX}$ simulated evapotranspiration worsened, i.e., R^2 decreased (0.61 to 0.42), RMSE increased (0.54 to 0.62 mm d^{-1}), and bias changed direction (0.09 to -0.09 mm d^{-1}). As evaporation is a highly parameterized process in CLASSIC, it likely needs to be re-parameterized to account for the SOX transpiration behaviour.

Plain Language Summary

Most terrestrial ecosystem models (TEMs) perform poorly during drought conditions in terms of simulating gross primary production (GPP), which is linked to their soil moisture stress (SMS) functions. Soil moisture stress functions implemented in TEMs empirically relate the effect of soil water stress on stomatal conductance. An alternative to SMS function is a plant hydraulics parameterization (e.g. Stomatal optimization based on Xylem hydraulics - SOX), which connects the soil-plant-atmosphere in a single continuum using plant hydraulic traits. In this study, we implemented SOX in the Canadian Land Surface Scheme Including biogeochemical Cycles (CLASSIC) TEM replacing its SMS function. The original CLASSIC and CLASSIC with the new plant hydraulics parameterization (CLASSIC$_{SOX}$) were evaluated at eight boreal forest flux tower sites in North America. CLASSIC$_{SOX}$ improved GPP compared to CLASSIC, especially during drought conditions. However, CLASSIC$_{SOX}$ needs further refinement for evapotranspiration by re-parameterizing the evaporation scheme corresponding to SOX transpiration. Overall, plant hydraulics parameterization improved simulated GPP while using fewer parameters and increased ecological realism compared to the SMS function.

Keywords: Terrestrial ecosystem model, plant hydraulics, drought conditions, boreal forest, carbon and water fluxes, soil moisture stress

1 Introduction

Intensification of the hydrological cycle and the projected increase in the frequency and severity of extreme events such as droughts challenge our ability to predict land-atmosphere interactions (Rahmstorf & Coumou, 2011; He et al., 2017; Anderegg et al., 2019; Miralles et al., 2019). Most TEMs, including the Canadian Land Surface Scheme Including biogeochemical Cycles (CLASSIC; Melton et al. (2020)), use an empirical soil moisture stress (SMS) function in their optimality-based photosynthesis scheme to constrain carbon assimilation through photosynthesis (A) and stomatal conductance (g_s) (e.g., Cox et al., 1998; Medlyn et al., 2016; Best et al., 2011; Clark et al., 2011; Ronda et al., 2001). However, SMS functions have only limited theoretical support (Medlyn et al., 2016; Anderegg & Venturas, 2020), and tend to underestimate gross primary production (GPP) during

natural and experimental drought conditions (Ukkola et al., 2016; Eller et al., 2018; Trugman et al., 2018). This limited skill has led to a growing demand for increased ecological realism in TEMs to improve model simulations under drought conditions, often addressed by replacing SMS functions with explicit representations of plant hydraulics (Kennedy et al., 2019; Eller et al., 2020; Sabot et al., 2020; Green et al., 2024; Paschalis et al., 2024). Stomatal conductance quantifies stomatal opening and thus is a key parameter that connects the terrestrial carbon and water cycles (Sellers et al., 1996; Cox et al., 1999). Water moves from soils to plants through the rhizosphere and the plant hydraulic system, which is composed primarily of xylem tracheary elements (Williams et al., 1996). Once the water reaches the leaves, it enters the atmosphere through the stomata by evaporation, thus connecting the soil-plant-atmosphere continuum (Williams et al., 1996). Stomatal conductance responds dynamically to soil moisture, atmospheric CO_2 concentration (c_a), and meteorological conditions, allowing plants to regulate carbon gain and water loss over a wide range of environmental conditions (Grantz, 1990; Field et al., 1995; Buckley, 2019). Several plant photosynthetic and hydraulic traits, such as xylem hydraulic conductance and vulnerability to embolism, are coupled with stomatal regulation (Ethier et al., 2006; Brodribb & Jordan, 2008; Martínez-Vilalta et al., 2014; Martin-StPaul et al., 2017).

In addition to implementing soil moisture stress through SMS functions, optimality-based photosynthesis schemes can simulate stomatal conductance response to environmental conditions without explicitly including plant hydraulics (Cowan & Farquhar, 1977; Leuning, 1995; Medlyn et al., 2011). Optimality-based photosynthesis schemes simulate stomatal conductance response to the environment by maximizing an objective function (Dewar et al., 2009; Prentice et al., 2014; Buckley, 2017; Franklin et al., 2020). Cowan and Farquhar (hereafter CF) (Cowan & Farquhar, 1977) introduced an approach for optimizing the stomatal conductance response, which has been adopted in many TEMs (Medlyn et al., 2001, 2011; Melton et al., 2020). The objective function (A-λT) in the CF approach maximizes carbon gain and postulates that plants try to maintain a constant marginal water use efficiency, λ. The CF approach effectively simulates the stomatal conductance response to meteorological conditions based upon available water (Farquhar et al., 1980) and has laid the foundation for several widely used photosynthesis schemes (Jacobs, 1994; Leuning, 1995; Medlyn et al., 2011). However, CF simulates an increase in g_s under an increase in c_a, a response contrary to most observations (Mott, 1988; Medlyn et al., 2001). Furthermore, λ in the CF approach is not linked with plant hydraulic traits, which form the basis for how plants transport water from their roots to stomata (Buckley, 2017). Stomatal conductance can be modelled using photosynthesis schemes that consider both structural and functional plant traits within physiological constraints (Dewar, 2010; Sabot et al., 2022). Various photosynthesis schemes based on plant hydraulics have been proposed in the last decade to overcome the limitations of empirical functions and optimality-based photosynthesis schemes by directly accounting for the loss of capacity to transport water from soil to leaf during drought conditions (Mencuccini, Manzoni, & Christoffersen, 2019; Sabot et al., 2022). Hydraulics-based photosynthesis schemes use plant hydraulic traits to produce realistic stomatal conductance response to environmental conditions (Choat et al., 2012; Manzoni, Vico, Katul, et al., 2013; Lin et al., 2015; Sperry et al., 2017; Eller et al., 2018; Mencuccini, Manzoni, & Christoffersen, 2019; Wang et al., 2019; Eller et al., 2020; Sabot et al., 2020). One example of a hydraulics-based photosynthesis scheme is the Stomatal Optimization based on Xylem hydraulics (SOX; Eller et al. (2018)). In brief, SOX is based on the Sperry et al. (2017) approach but incorporates a numerical routine similar to the PGEN model (a leaf-scale model of photosynthesis, respiration, transpiration, stomatal conductance, and energy balance; Friend, 1995). The SOX approach uses three xylem hydraulic parameters to optimize the product of A and the cost associated with the xylem hydraulic conductance loss, which is represented as a function of water potential (Ψ) (Eller et al., 2018).

Limited research has been conducted to adequately simulate g_s using plant hydraulics in the boreal biome due to cold winters, summer droughts, and scarcity of in-situ plant

hydraulic observations (Manzoni, Vico, Porporato, & Katul, 2013; Lin et al., 2015; Sabot et al., 2020; Lambert et al., 2022). In this study, we integrated SOX with CLASSIC to simulate g_s using plant hydraulics and stomatal optimization, resulting in CLASSIC$_{SOX}$. We evaluated both CLASSIC and CLASSIC$_{SOX}$ at eight boreal forest flux tower sites in North America (Qu, Roy, Melton, Black, et al., 2023). By enhancing the ecological realism in CLASSIC$_{SOX}$, our goal was to improve the performance of CLASSIC regarding daily evapotranspiration (ET) and GPP. To meet our goal, our two objectives were to:

1. examine the response of g_s to environmental conditions in SOX compared to the SMS function used in CLASSIC and
2. evaluate the performance of CLASSIC$_{SOX}$ compared to CLASSIC against observation-based estimates of daily GPP and ET with a focus on drought conditions identified with the Palmer drought severity index (Palmer, 1965; Wells et al., 2004).

2 Materials and Methods

2.1 The Canadian Land Surface Scheme Including biogeochemical Cycles (CLASSIC)

CLASSIC is an open-source community model and successor to the Canadian Land Surface Scheme (CLASS) and the Canadian Terrestrial Ecosystem Model (CTEM) (Melton et al., 2020; Seiler et al., 2021). CLASSIC uses a photosynthesis scheme derived from Collatz et al. (1991, 1992) for C3 and C4 plants, calculating the maximum carbon assimilation rate allowed by light, RuBisCO, and electron transport capacity (Melton & Arora, 2016). The maximum catalytic capacity of RuBisCO (V_m, mol CO_2 m^{-2} s^{-1}) is calculated as:

$$V_m = \frac{V_{max} f_{25}(2.0) S_{root}(\theta) \times 10^{-6}}{[1 + e^{0.3(T_c - T_{high})}][1 + e^{0.3(T_{low} - T_c)}]} \tag{1}$$

where T_c (°C) is the canopy temperature, T_{low} (°C) and T_{high} (°C) are the plant functional type (PFT)-dependent lower and upper-temperature limits for photosynthesis, f_{25} is the standard Q_{10} function at 25 °C, and V_{max} is the PFT-dependent maximum rate of carboxylation by the RuBisCO enzyme (mol CO_2 m^{-2} s^{-1}). The constant 10^{-6} converts V_{max} from units of μmol CO_2 m^{-2} s^{-1} to mol CO_2 m^{-2} s^{-1}. The effect of soil moisture on carbon assimilation rate is introduced through a multiplier for V_m ($S_{root}(\theta)$, which is given as:

$$S_{root}(\theta) = \sum_{i=1}^{g} S(\theta_i) r_i \tag{2}$$

$$S(\theta_i) = [1 - [1 - \Phi_i]]^{\varrho} \tag{3}$$

where $S_{root}(\theta)$ is calculated by weighting $S(\theta_i)$ with the fraction of roots (r_i) in each soil layer, i, and ϱ is a PFT-specific sensitivity to soil moisture stress (Melton & Arora, 2016). Φ_i is the degree of soil saturation (wetness) and given as:

$$\Phi_i(\theta_i) = max\left[0, min\left(1, \frac{\theta_i - \theta_{i,wilt}}{\theta_{i,field} - \theta_{i,wilt}}\right)\right] \tag{4}$$

where θ_i is the volumetric soil moisture (m^3 m^{-3}) of the ith soil layer and $\theta_{i,field}$ and $\theta_{i,wilt}$ are the soil moisture at field capacity and wilting point, respectively.
CLASSIC employs the approach of Leuning (1995) for photosynthesis-canopy conductance coupling. Canopy conductance (g_c, mol m^{-2} s^{-1}) is calculated as a function of net photosynthesis rate ($G_{canopy,net}$, mol CO_2 m^{-2} s^{-1}), as below:

$$g_c = m\frac{G_{canopy,net} P_{atm}}{(c_s - \Gamma)} \frac{1}{(1 + VPD/VPD_o)} + bLAI \tag{5}$$

where m and b are fitting parameters. The value of m is: 9.0 (for needle-leaved trees), 12.0 (for other C3 plants), and 6.0 (for C4 plants), and the value of b is 0.01 and 0.04 for C3 and C4 plants, respectively. Surface atmospheric pressure is represented by P_{atm} (Pa). VPD is vapour pressure deficit (kPa), and parameter VPD_o is 2000 Pa for trees and 1500 Pa for crops and grasses. Γ is the CO_2 compensation point (CO_2 partial pressure where photosynthetic uptake equals the leaf respiratory losses), and LAI is leaf area index (m^2 of leaf m^{-2} of ground). The CO_2 partial pressure at the leaf surface, c_s, is calculated as:

$$c_s = c_{ap} - \frac{1.37 G_{canopy.net} P_{atm}}{g_b} \tag{6}$$

where c_{ap} is CO_2 atmospheric partial pressure (Pa) and g_b is the aerodynamic conductance (mol CO_2 m^{-2} s^{-1}). Intercellular CO_2 concentration, c_i (Pa), is calculated as:

$$c_i = c_s - \frac{1.65 G_{canopy,net} P_{atm}}{g_c} \tag{7}$$

as the calculations of c_i and $G_{canopy,net}$ depend on each other; the equations are solved iteratively for photosynthesis-canopy conductance coupling. The initial value of c_i is the value from the previous time step or, lacking that, is taken as $0.7c_{ap}$. For more details on CLASSIC configuration and parameter values, see Melton and Arora (2016) and Qu, Roy, Melton, Baltzer, et al. (2023).

2.2 Stomatal Optimization based on Xylem hydraulics

Over the last three decades, the ecological realism in various TEMs has been enhanced through explicit plant hydraulics parameterizations (Williams et al., 1996; Hickler et al., 2006; Bonan et al., 2014; Kennedy et al., 2019; Eller et al., 2020; Sabot et al., 2022). Often, the motivation to implement an explicit plant hydraulics parameterization was to address the overestimation of drought impacts on GPP due to SMS functions (Eller et al., 2018, 2020). We considered four different plant hydraulics parameterizations for inclusion in CLASSIC. Hickler et al. (2006) introduced plant hydraulics in the LPJ-DGVM model and used the hypothesis of maximizing conductance based on the xylem vulnerability curve (Tyree & Sperry, 1989; Tyree et al., 1994; Sperry et al., 1998). The LPJ-DGVM approach has six parameters from three plant structures (leaf, stem, root) and is of relatively high complexity. Bonan et al. (2014) implemented the soil-plant-atmosphere model with CLM4.5 (SPA; Williams et al. (1996, 2001)) as a photosynthesis scheme based on optimized water use efficiency and constrained leaf water potential. This implies a strict isohydric behaviour (isohydric plants maintain constant leaf water potential during drought and non-drought conditions by controlling stomatal conductance and transpiration.) similar to the LPJ-DGVM approach of Hickler et al. (2006). The plant hydraulic stress (PHS) approach implemented in CLM5.0 (Kennedy et al., 2019) included vapour pressure deficit (VPD) in its water stress function, not considered by Bonan et al. (2014). High VPD causes an increase in the water potential gradient between the soil and the atmosphere with consequences for stomatal conductance response. Due to the projected increase of VPD associated with global warming, it will be essential to represent VPD in plant hydraulics parameterizations for stomatal optimization (Seager et al., 2015; Ficklin & Novick, 2017). The PHS approach used plant hydraulics with soil moisture stress, which is a highly detailed parameterization in three plant structures (leaf, stem, and roots) and involves four parameters (Kennedy et al., 2019). Eller et al. (2018, 2020) introduced the SOX approach with numerical optimization and analytical approximation. The plant hydraulics parameterization introduced through SOX considers how both VPD and soil water potential regulate plant hydraulic conductance in a single compartment (Section 2.3). Sabot et al. (2022) compared several empirical and plant hydraulics parameterizations for photosynthesis using a single TEM. The SOX numerical approach has been identified as being among the most effective plant hydraulics parameterizations during drought and non-drought conditions (Wang et al., 2020; Sabot et al., 2022).

We used three criteria to select an appropriate plant hydraulics parameterization for inclusion in CLASSIC: 1) a small number of parameters to limit issues related to parameter uncertainty and equifinality, 2) moderate complexity to match the general approach of CLASSIC, and 3) potential applicability across diverse landscapes (Kyker-Snowman et al., 2022). Based upon these criteria, we decided to integrate SOX with CLASSIC due to its relatively parsimonious parameterization compared to the SMS function in CLASSIC (Eller et al., 2018; Melton et al., 2020). In addition, SOX is of reasonable complexity and previous studies demonstrated its applicability in tropical and temperate biomes (Eller et al., 2018, 2020).

2.3 CLASSIC with Stomatal Optimization based on Xylem hydraulics (CLASSIC$_{SOX}$)

Calculation of g_c, assimilation (A), and transpiration (T) through SOX requires five steps: 1) calculation of SOX parameters using wood density (WD; Text A1, A2), 2) calculation of A using c_i values, 3) calculation of a cost function based on xylem hydraulic conductance loss (k_{cost}) using equations 12, 13, and 14, 4) calculation of optimum c_i using A and k_{cost} (equation 15), and 5) calculation of g_c, and T using optimum c_i and A. The SOX approach uses changes in xylem hydraulic conductance to find the optimal stomatal conductance (g_s, mol m^{-2} s^{-1}) value for the current environmental conditions (Eller et al., 2018). The SOX approach calculates optimal g_s by maximizing the product of carbon assimilation (A, mol m^{-2} s^{-1} and (k_{cost}) using a numerical optimization algorithm (Friend, 1995; Eller et al., 2018). The SOX approach can be used with any TEM that calculates A using c_i (Pa) and meteorological conditions. Here, SOX is implemented into CLASSIC via its photosynthesis scheme. Stomatal conductance and transpiration (T, mol H_2O m^{-2} s^{-1}) are derived by using A, c_i, c_a (Pa), and VPD as:

$$g_s = \frac{A}{c_a - c_i} \tag{8}$$

$$T = 1.6 g_s VPD \tag{9}$$

where the value 1.6 represents the ratio between water vapour and CO_2 diffusion in the air.

Using Darcy's Law, leaf water potential (Ψ_l, MPa) is calculated using T assuming steady-state conditions (without considering stored water in plants for T):

$$\Psi_l = \Psi_{l,pd} - \frac{T}{k_{sl}} \tag{10}$$

where k_{sl} is the xylem hydraulic conductance from soil to leaf (mol m^{-2} s^{-1} MPa^{-1}), and $\Psi_{l,pd}$ is the predawn leaf water potential (MPa) calculated using root water potential (Ψ_r, MPa) reduced by the water potential gradient induced by canopy height (h, m):

$$\Psi_{l,pd} = \Psi_r - h\rho g \times 10^{-6} \tag{11}$$

where ρ is the density of water (1000 kg m^{-3}), g is the acceleration due to gravity (9.8 m s^{-2}), and 10^{-6} is for unit conversion from Pa to MPa. Following a simple and parameter parsimonious approach for SOX, we assumed root water potential (Ψ_r) is approximately equal to the soil water potential (Ψ_s, MPa) ($\Psi_r \approx \Psi_s$).

As Ψ_l and k_{sl} depend on each other for their computation, thus a drought-induced reduction in Ψ_l leads to a decrease in k_{sl}, and vice-versa (equation 10; Sperry & Tyree, 1988). The inverse polynomial function from Manzoni, Vico, Katul, et al. (2013) is used to represent k_{sl}:

$$k_{sl} = k_{sl,max}\left[1 + \left(\frac{\Psi_{l,mid}}{\Psi_{50}}\right)^a\right]^{-1} \tag{12}$$

where the parameter Ψ_{50} is the water potential at 50 % loss of maximum hydraulic conductance (i.e., $0.5k_{sl,max}$), and a is the vulnerability curve parameter which controls the

shape of the hydraulic conductance loss curve with decreasing Ψ_l. The parameter a is calculated using Ψ_{50} following empirical relationship (Text A1, Christoffersen et al., 2016). In-situ observations of Ψ_{50} for boreal forests are scarce. Thus, WD (g cm^{-3}) was used to calculate Ψ_{50} based on an empirical relationship (Text A1, Christoffersen et al., 2016). Wood density was also used to calculate $k_{sl,max}$ based on an empirical relationships (Text A2, Savage et al., 2010; Christoffersen et al., 2016). This approach decreases the number of required parameters for SOX to only one (WD). CLASSIC$_{SOX}$ uses k_{sl} from the previous time-step to calculate the Ψ_l and determines k_{sl} for the current time-step using equations 10 to 12.

Following Eller et al. (2018), we assume the gradual drop of water potential in plants using the middle value of the Ψ_l and $\Psi_{l,pd}$ ($\Psi_{l,mid}$):

$$\Psi_{l,mid} = \frac{\Psi_{l,pd} + \Psi_l}{2} \tag{13}$$

For the cost of stomatal opening (k_{cost}), the k_{sl} is calculated using equation 12 and normalized with the $k_{sl,max}$:

$$k_{cost} = \frac{k_{sl}}{k_{sl,max}} \tag{14}$$

The SOX approach maximizes the product of A and k_{cost} as a function of c_i by evaluating it in the interval (0, c_a) as used by others (Friend, 1995; Eller et al., 2018). For the maximum value of the product of A and k_{cost}, the optimum c_i ($c_{i,opt}$) can be found at:

$$\frac{\partial(A.k_{cost})}{\partial(c_i)} = 0 \tag{15}$$

$c_{i,opt}$ is then used to calculate optimum A, g_s, T, and Ψ_l using the photosynthesis scheme (Collatz et al., 1991, 1992; Melton & Arora, 2016) and equations 8, 9, and 10.

We calculated soil liquid fraction (between 0 to 1, unitless) to constrain g_c, A, and R_{mL} during freezing conditions.

$$SL_{frac} = \frac{\theta_{liq}}{\theta_{liq} + \theta_{ice}} \tag{16}$$

$$g_c = g_c \times SL_{frac} \tag{17}$$

$$A = A \times SL_{frac} \tag{18}$$

$$R_{mL} = R_{mL} \times SL_{frac} \tag{19}$$

For the implementation in CLASSIC, SOX then replaces the CLASSIC calculations found in equations 1 to 7 expressing SMS function ($S_{root}(\theta)$) and computes g_c from plant hydraulic traits and meteorological variables using equations 8 to 15 (Fig. 1).

2.4 Parsimonious parametrization

Our implementation of SOX in CLASSIC (CLASSIC$_{SOX}$) is a parameter parsimonious approach compared to the SMS function in the original version of CLASSIC. Three additional parameters are needed by SOX: Ψ_{50}, $k_{sl,max}$, and canopy height (h). CLASSIC updates h daily based upon growing conditions for the vegetation. Using empirical relationships, we calculated $k_{sl,max}$ from Ψ_{50} and WD (Savage et al., 2010; Christoffersen et al., 2016; Eller et al., 2018). Thus, the total parameters in CLASSIC$_{SOX}$ was one (WD) compared to four in CLASSIC (ρ for PFT-specific sensitivity to soil moisture stress, equation 3; m, b, and V_o for photosynthesis and canopy conductance coupling, equation 5). The fewer parameters in CLASSIC$_{SOX}$ compared to CLASSIC can be advantageous for avoiding problems related to parameter uncertainty and equifinality.

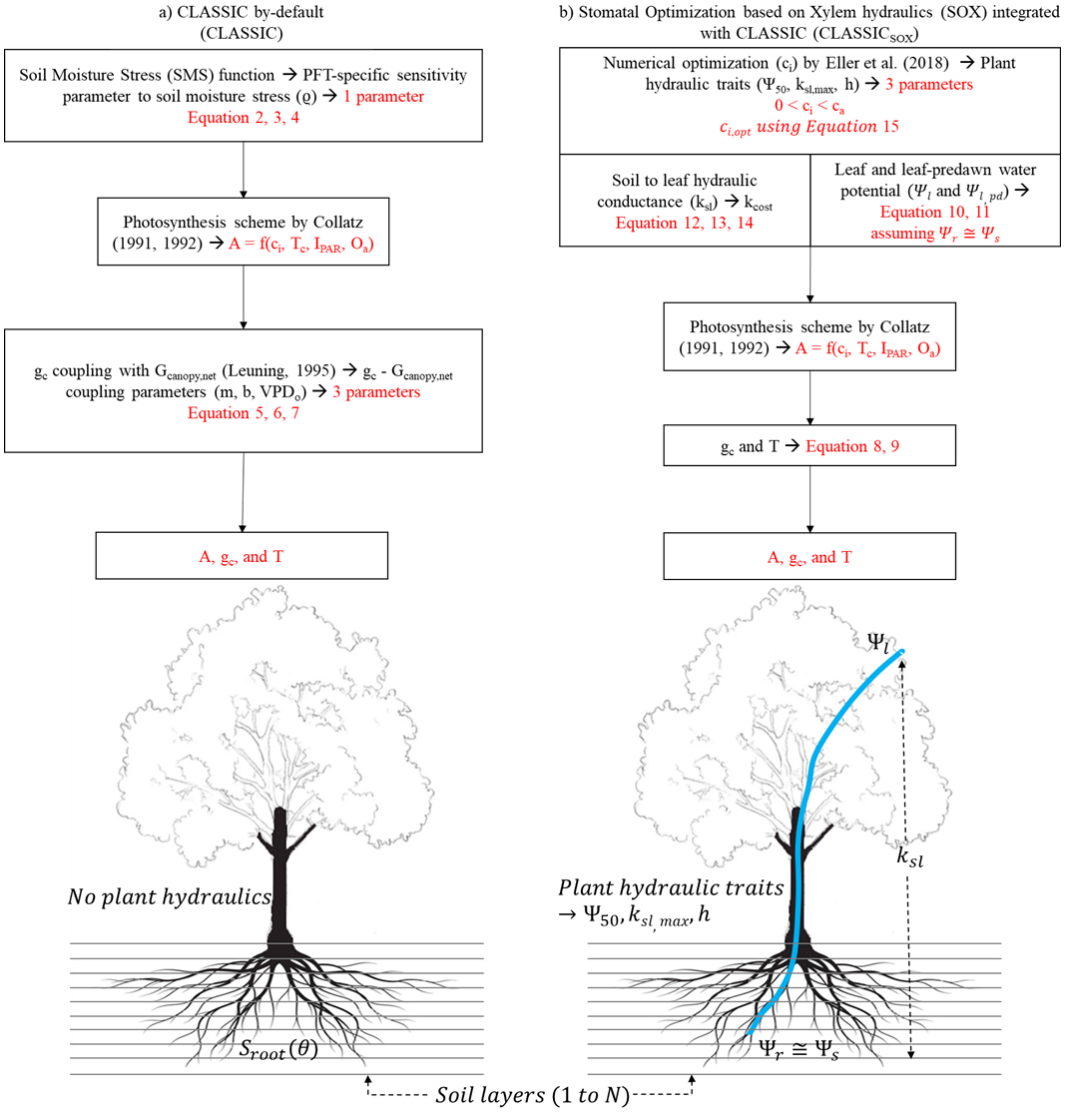

Figure 1. Equations and parameters used to calculate canopy conductance (g_c) using a) CLASSIC and b) CLASSIC$_{SOX}$. All symbols are defined in the model explanation sections 2.1 and 2.3 except air O_2 concentration (O_a). In CLASSIC$_{SOX}$, the blue line shows a water channel from soil to plants and then to the atmosphere using plant hydraulic traits and soil (Ψ_s) and leaf water potential (Ψ_l).

2.5 Boreal forest flux tower sites

We used eddy covariance measurements from eight boreal forest flux tower sites with a total of 65 site years (ranging from 1994-2019) to evaluate fluxes simulated with CLASSIC and CLASSIC$_{SOX}$ (Fig. S1, Table S1). Site characteristics, meteorological, and water and carbon flux data used for model parameterization, forcing and evaluation were obtained from a recently compiled boreal forest model benchmarking dataset for North America (Qu, Roy, Melton, Black, et al., 2023, See Table S1 for further details about the sites), respectively.
Wood density data for all Canadian sites was obtained from the National Forest Inventory archives (NFI, accessed 08 25, 2022). For the three Alaskan sites (US-BZS, US-Prr, US-Uaf), the WD for black spruce is assumed to be the same as the Canadian boreal forest sites. For evergreen needle-leaf (ENF, black spruce) trees, the WD is 0.332 g cm^{-3} for all sites except CA-Qfo, where it is 0.444 g cm^{-3} due to higher aridity index (AI). The western boreal biome had a lower AI (i.e., drier) compared to the higher AI (i.e., more humid) eastern boreal biome (Fig. S1; Zomer et al., 2022). For deciduous needle-leaf (DNF, tamarack) trees at CA-Obs, WD is 0.267 g cm^{-3}. For other PFTs (evergreen broad-leaf shrubs (EBS), deciduous broad-leaf shrubs (DBS), and C3 grass (C3G)) at all sites, the plant hydraulic parameters were used following Eller et al. (2020).

2.6 Experimental design

Four experiments are conducted (Table 1), each with a different model configuration. Experiments 1 and 2 are stand-alone outside of CLASSIC, while experiments 3 and 4 are based on CLASSIC. The experiments are: 1) CLASSIC's SMS function and photosynthesis scheme using constant meteorological conditions (Section 2.1, Table S2), 2) SOX approach using constant meteorological conditions (Section 2.3, Table S2), 3) CLASSIC (Section 2.1), and 4) CLASSIC with SOX implemented (CLASSIC$_{SOX}$, Section 2.3). Experiments 3 and 4 (Table 1) used the same initial conditions after spinning up the model using site-level meteorological forcing data for 200 years at each site.

Table 1. Experimental Design. All four experiments used the same photosynthesis scheme implemented in Canadian Land Surface Scheme Including biogeochemical Cycles (CLASSIC; Collatz et al., 1991, 1992). Constant and observed meteorological conditions are used as forcings in the model. SMS represents Soil Moisture Stress function and SOX represents Stomatal Optimization based on Xylem hydraulics.

Experiments	SMS	SOX	CLASSIC model	constant meteorology	observed meteorology
1- SMS	Yes	No	No	Yes	No
2- SOX	No	Yes	No	Yes	No
3- CLASSIC	Yes	No	Yes	No	Yes
4- CLASSIC$_{SOX}$	No	Yes	Yes	No	Yes

2.7 Model evaluation

We examined the response of g_s in experiments 1 (SMS) and 2 (SOX) to constant meteorological conditions (T_c, VPD, incident photosynthetically active radiation measured as photosynthetic photon flux density (I_{PAR}, μmol m^{-2} s^{-1})), c_a, and Ψ_s while varying the SOX parameters. The canopy conductance response to site-level meteorological conditions, c_a, and Ψ_s was also examined at all eight study sites for CLASSIC and CLASSIC$_{SOX}$. The results from experiments 3 and 4 (CLASSIC and CLASSIC$_{SOX}$, respectively) were evaluated against daily net ecosystem exchange-derived GPP (here-

after NEE-derived GPP) and ET obtained from eddy covariance measurements. Coefficient of determination (R^2), root mean square error (RMSE), and bias describe the model results by season (spring: March-April-May [MAM], summer: June-July-August [JJA], and autumn: September-October-November [SON]) and all seasons combined (All). The Palmer drought severity index (PDSI; Palmer, 1965; Wells et al., 2004) was used to identify drought conditions based on observed meteorological conditions at the flux tower sites (Fig. S2). The PDSI has seven categories with increasing water stress: wet periods (W; PDSI $\geq$ 0.50), normal conditions (N; 0.50 > PDSI > -0.50), incipient drought (A; -0.5 $\geq$ PDSI > -1.0), mild drought (B; -1.0 $\geq$ PDSI > -2.0), moderate drought (C; -2.0 $\geq$ PDSI > -3.0), severe drought (D; -3.0 $\geq$ PDSI > -4.0), and extreme drought (E; PDSI $\leq$ -4.0) (Wells et al., 2004). Two groups were created using the PDSI categories to plot and compare the results between drought (C, D, and E) and non-drought conditions (W, N, A, and B). Five sites (CA-Obs, CA-Man, CA-Qfo, US-BZS, US-Uaf) experienced drought conditions during the available observational periods (Fig. S2). The results for drought and non-drought conditions were plotted and compared with statistics between outputs from CLASSIC and CLASSIC$_{SOX}$ to evaluate the impact of replacing SMS function by SOX during drought conditions.

3 Results

3.1 Experiments 1 (SMS) and 2 (SOX)

Stomatal conductance response to changes in I_{PAR}, c_a, T_c, VPD, and Ψ_s for Experiment 1 (SMS) and Experiment 2 (SOX) with minimum, average, and maximum WD is shown in figure 2. SOX simulates increasing g_s and decreasing Ψ_l with increasing I_{PAR} (Fig. 2a, b). The response curves become more shallow as WD decreases (Fig. 2a, b). The slope of g_s with respect to increasing I_{PAR} for SOX is lower than the SMS function, which makes g_s higher at low I_{PAR} and slightly lower at high I_{PAR} (Fig. 2a). SOX simulates decreasing g_s and increasing Ψ_l with increasing c_a and WD, which can be corroborated by equation 8-10 (Fig. 2c, d). The SMS function simulates decreasing g_s with increasing c_a, similar to SOX curve of maximum WD (Fig. 2c). The response of g_s to T_c for SOX and SMS function is regulated by the relationship between V_m and T_c in the photosynthesis scheme (equation 1), resulting in higher g_s and lower Ψ_l at higher temperatures (Fig. 2e,f).
The stomatal conductance response to atmospheric demand represented by VPD resulted in decreasing g_s and Ψ_l for SOX and the SMS function as the atmosphere becomes drier with increasing VPD (Fig. 2g,h). In CLASSIC, g_s is higher (0.25 < VPD (kPa) < 5) and lower (0.25 > VPD (kPa) > 5) than SOX with maximum WD (Fig. 2g). The g_s for lower WD curves (0.18 and 0.35 g cm^{-3}) is lower for SOX than CLASSIC (Fig. 2g). In SOX, g_s and Ψ_l decreases with decreasing Ψ_s (Fig. 2i, j). The response of g_s to Ψ_s for SOX is more pronounced than for each of the meteorological variables due to higher g_s compared to the SMS function at low Ψ_s (Fig. 2i, j).
The relationship between g_c and I_{PAR}, c_a, T_c, VPD, and Ψ_s highlights the increase in g_c for CLASSIC$_{SOX}$ at all sites (Fig. S3). Overall g_c increased from 0.15 mol C m^{-2} s^{-1} with CLASSIC to a maximum of 0.4 mol C m^{-2} s^{-1} for CLASSIC$_{SOX}$ (Fig. S3).

3.2 Evaluation of CLASSIC$_{SOX}$

CLASSIC$_{SOX}$ simulated higher daily GPP than CLASSIC at all sites (Fig. 3, S4a, S5). During peak summer (around July), CLASSIC$_{SOX}$-simulated GPP was closer to observed NEE-derived GPP compared to CLASSIC (Fig. 3). At the two Alaskan sites, US-BZS and US-Uaf, both model versions underestimated the simulated GPP during peak summer. Even though CLASSIC$_{SOX}$ simulated higher GPP than CLASSIC at US-BZS and US-Uaf, both versions of CLASSIC considerably underestimated GPP compared to the NEE-derived GPP (Fig. 3f, h, S5f, h). The bias between CLASSIC$_{SOX}$ and NEE-

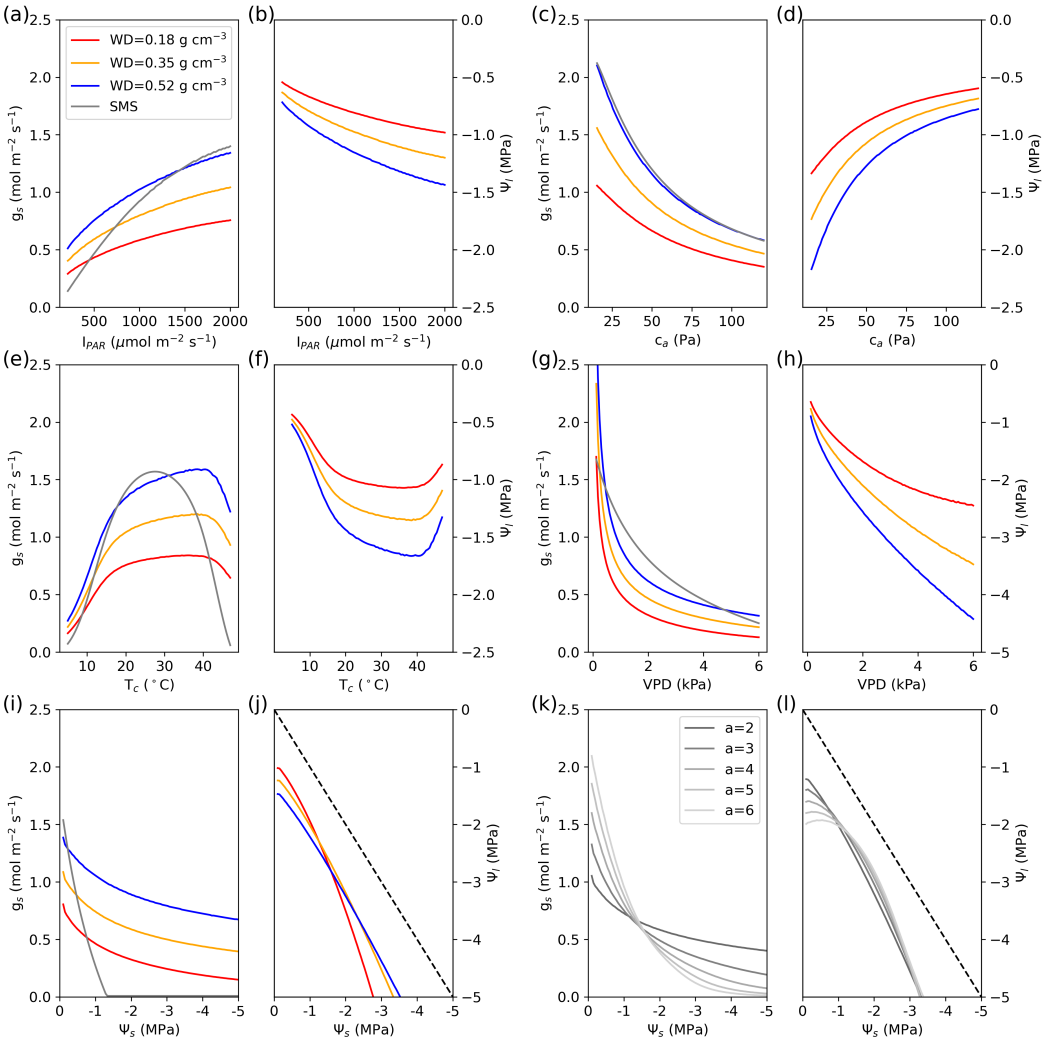

Figure 2. Response functions for stomatal conductance (g_s) and leaf water potential (Ψ_l) with meteorological variables (incident photosynthetically active radiation (I_{PAR}), canopy temperature (T_c), vapour pressure deficit (VPD)), atmospheric CO_2 concentration (c_a), and soil water potential (Ψ_s) for experiment 1 and 2. All other input variables and parameters are kept constant at their default values (Table S2). Canopy water potential at 50 % of hydraulic conductance loss (Ψ_{50}) and vulnerability curve parameter (a) values for the respective wood density (WD) values are: WD = 0.18 g cm^{-3}, Ψ_{50} = -1.59 MPa, a = 2.32; WD = 0.35 g cm^{-3}, Ψ_{50} = -2.60 MPa, a = 2.05; WD = 0.52 g cm^{-3}, Ψ_{50} = -4.03 MPa, a = 1.84. The WD values correspond with the minimum (0.18 g cm^{-3}), average (0.35 g cm^{-3}), and maximum (0.52 g cm^{-3}) from the NFI dataset over the Canadian boreal forest (NFI, accessed 08 25, 2022). SMS represents the CLASSIC's soil moisture stress function.

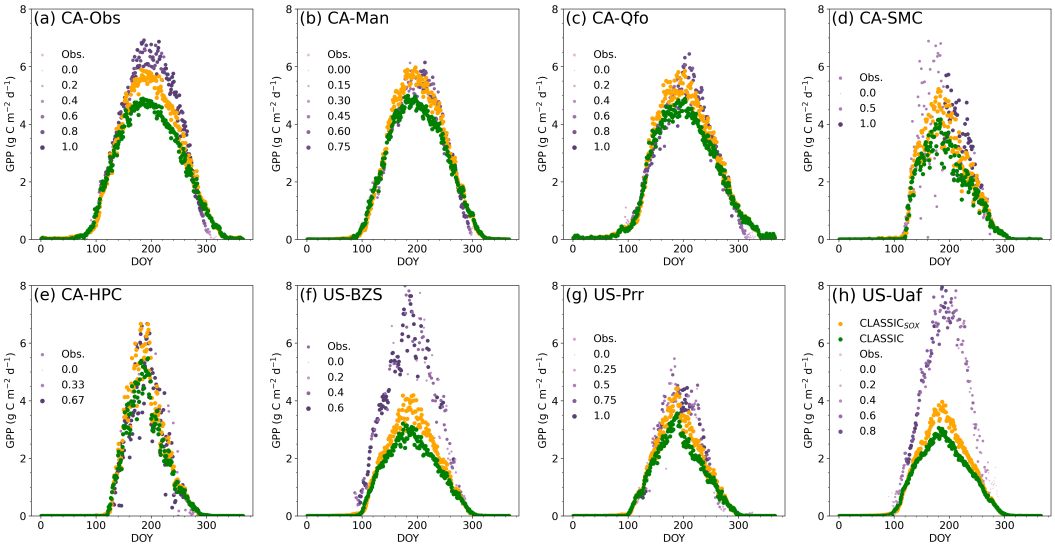

Figure 3. Mean annual observed NEE-derived gross primary production (GPP) compared to mean annual simulated daily GPP with CLASSIC$_{SOX}$ and CLASSIC. The size and hue of the NEE-derived GPP dots represent the percentage of observations available across possible days for the site years with larger and darker dots representing periods with a greater number of observations. DOY is day-of-year.

derived GPP during peak summer decreased for CA-Obs and CA-SMC than CLASSIC (Fig. 3a, d, S5a, d), but CLASSIC$_{SOX}$ adequately matched the observations at the remaining sites (Fig. 3b, c, e, and g). At most sites, R^2, RMSE, and bias improved using CLASSIC$_{SOX}$ compared to CLASSIC (Fig. S5). A combined scatterplot for all sites revealed improved statistics for GPP, i.e., R^2 increased from 0.51 to 0.59 (16 %), while RMSE and bias decreased from 1.85 to 1.54 g C m^{-2} d^{-1} (17 %) and -0.99 to -0.58 g C m^{-2} d^{-1} (41 %), respectively, between CLASSIC$_{SOX}$ and CLASSIC against NEE-derived GPP (Fig. S4a). The seasonal (MAM, JJA, SON, and All) R^2, RMSE, and bias showed that MAM and SON have better results compared to JJA (Fig. S7a-c, 3). Overall, cumulative GPP increased from 23.54 kg C m^{-2} to 27.14 kg C m^{-2} for eight sites (65 site-years) compared to NEE-derived cumulative GPP of 32.12 kg C m^{-2}, which is 15 % (42 % of the total difference between CLASSIC and observations) increased results using CLASSIC$_{SOX}$ compared to CLASSIC.

For ET, three sites (CA-Obs, CA-Man, and CA-Qfo) showed underestimation at peak summer with a negative bias and lower R^2 for CLASSIC$_{SOX}$ than CLASSIC (Fig. 4a-c, S6a-c). However, the remaining sites showed similar results for CLASSIC$_{SOX}$ and CLASSIC (Fig. 4d-h, S6d-h). For all sites combined, the R^2 decreased from 0.61 to 0.42 (31 %), RMSE increased from 0.54 to 0.62 mm d^{-1} (15 %), and bias changed from overestimation to underestimation (0.09 to -0.09 mm d^{-1}) between CLASSIC and CLASSIC$_{SOX}$ when compared against observations (Fig. S4b). The seasonal (MAM, JJA, SON, and All) R^2, RMSE, and bias showed a weaker relationship for CLASSIC$_{SOX}$ at CA-Obs, CA-Man, and CA-Qfo than CLASSIC against observations (Fig. 4a-c, S7d-f). However, the remaining sites showed approximately similar seasonal statistics for CLASSIC$_{SOX}$ and CLASSIC (Fig. 4d-h, S7d-h).

For all sites combined, the GPP-ET relationship for flux tower observations, CLASSIC$_{SOX}$, and CLASSIC showed increased R^2 (from 0.21 to 0.42) for CLASSIC than CLASSIC$_{SOX}$ compared to the observed R^2 of 0.61. However, the slope and intercept increased (from 1.08 to 1.12, and 1.29 to 1.86, respectively) for CLASSIC$_{SOX}$ than CLASSIC compared

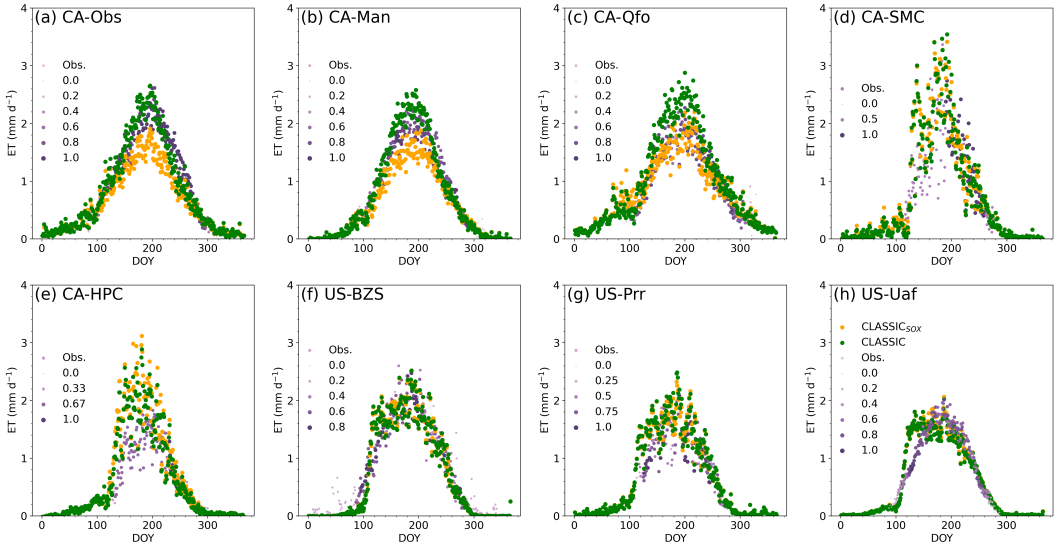

Figure 4. Mean annual observed evapotranspiration (ET) compared to mean annual simulated daily ET with CLASSIC$_{SOX}$ and CLASSIC. The size and hue of the ET dots represent the percentage of observations available across possible days for the site years with larger and darker dots representing periods with a greater number of observations. DOY is day-of-year.

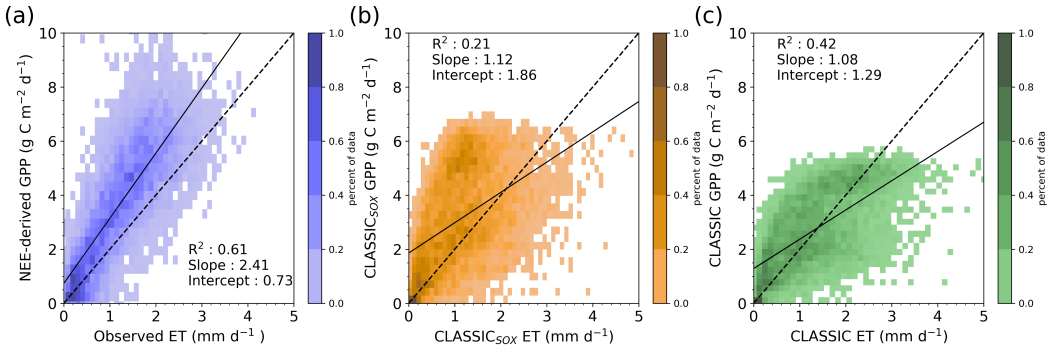

Figure 5. Kernel density plots describing the relationship between gross primary production (GPP) and evapotranspiration (ET) at all sites for flux tower observations (a), CLASSIC$_{SOX}$ (b), and CLASSIC (c). As a visual guide, the black dotted line is the 2:1 line between GPP and ET (GPP = 2 × ET).

to the observed slope and intercept of 2.41 and 0.73, respectively (Fig. 5). The underestimated ET for CLASSIC$_{SOX}$ is reflected in the GPP-ET relationship with decreased R^2 (Fig. 5). The higher intercept for CLASSIC$_{SOX}$ shows higher evaporation (when T is zero on the Y-axis) than CLASSIC and observations (Fig. 5b).

3.3 Model responses during drought

CLASSIC$_{SOX}$ simulated GPP considerably better, under drought and non-drought conditions, than CLASSIC (Fig. 6a,b). The statistics for CLASSIC$_{SOX}$ compared to CLASSIC were also higher for the drought than non-drought conditions, i.e., R^2 increased from 0.51 to 0.60, while RMSE and bias decreased from 1.79 to 1.46 g C m^{-2} d^{-1} and -0.97 to -0.53 g C m^{-2} d^{-1}, respectively (Fig. 6a). Under non-drought conditions, the statistics for CLASSIC$_{SOX}$ compared to CLASSIC were comparatively lower, i.e., R^2 increased from 0.51 to 0.58, while RMSE and bias decreased from 1.87 to 1.56 g C m^{-2} d^{-1} and -1.0 to -0.59 g C m^{-2} d^{-1}, respectively (Fig. 6b). For ET, similar to what can be seen in figure 4, CLASSIC$_{SOX}$ performance when compared for the drought and non-drought conditions showed poorer with observations than CLASSIC (Fig. 6c,d). Under drought conditions CLASSIC$_{SOX}$ compared to CLASSIC saw ET R^2 decreased from 0.60 to 0.43, while RMSE and bias increased from 0.53 to 0.59 (mm d^{-1}) and 0.08 (overestimation) to -0.14 (mm d^{-1}) (underestimation). Under non-drought conditions, ET R^2 decreased from 0.61 to 0.41, RMSE and bias increased from 0.55 to 0.63 (mm d^{-1}) and 0.09 (overestimation) to -0.08 (mm d^{-1}) (underestimation).

4 Discussion

Our study focused on two objectives which will be discussed here: 1) to examine the response of g_s to environmental conditions in SOX compared to the SMS function used in CLASSIC, and 2) to evaluate the performance of CLASSIC$_{SOX}$ compared to CLASSIC against observation-based estimates of daily GPP and ET with a focus on drought conditions identified with the PDSI.

Stomatal conductance (g_s) response for SOX (for cases of higher and lower WD) and the SMS function of CLASSIC to each environmental condition is essential to understand before site-level analysis (Experiments 1 and 2, Fig. 2). The stomatal conductance response to T_c for SOX is not following the parabolic curve of the SMS function at higher T_c; SOX shows an effect of hydraulic-induced stomatal closure at higher T_c varying with WD (where the VPD would get higher at higher T_c, which would increase T and Ψ_l and make the stomata close later for higher WD than SMS function) (Fig. 2e, f). The stomatal conductance response to increasing VPD in SOX for plants vulnerable to cavitation (characterized by low WD and high Ψ_{50}) is captured through a reduction in their hydraulic conductance, even at high Ψ_l, which results in a lower g_s compared to the SMS function (Fig. 2g, h). Plants with a higher WD (and thus a lower Ψ_{50}) can maintain more open stomata in SOX despite higher atmospheric demand for water (higher VPD), leading to a higher g_s, T, hydraulic conductance, and lower Ψ_l (Fig. 2g, h). However, in the SMS function, the rate of decrease for g_s with respect to VPD is higher than the more gradual g_s decrease in SOX, which makes the SMS function simulated g_s higher for moderate atmospheric demand (VPD) than simulated by SOX (Fig. 2g, h). The higher g_s simulated by SOX at both high and low Ψ_s, shows that even at very low Ψ_s of -5 MPa under drought conditions (Fig. 2i), plants can continue photosynthesis and retain higher g_s for SOX compared to SMS function. Higher g_s is achieved by using the k_{sl} in SOX, which varies according to the plant hydraulic parameters and Ψ_s, instead of using the SMS function, which restricts photosynthesis earlier as the Ψ_s reaches the wilting point (Fig. 2i, j). For the combined effect of the meteorological variables (T_c, VPD, and I_{PAR}), c_a, and Ψ_s at all eight sites, g_c is simulated higher by CLASSIC$_{SOX}$ than CLASSIC (Fig. S3), which might be due to Ψ_s (considering its higher g_s for SOX) compared to other meteorological variables (Fig. 2).

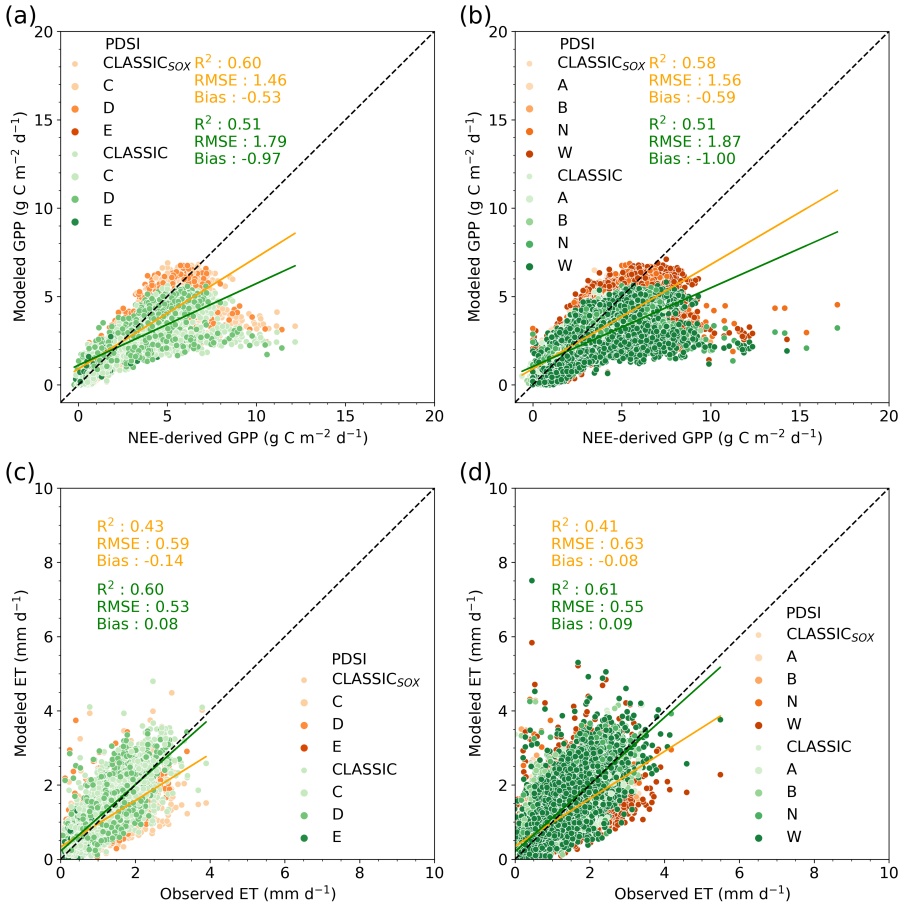

Figure 6. Model response to drought (a,c) and non-drought (b,d) categories for daily gross primary production (GPP, top row) and evapotranspiration (ET, bottom row). The drought categories are defined using the Palmer drought severity index (PDSI). Drought is categorized as extreme (E), severe (D), and moderate (C), while non-drought conditions include mild (B), incipient (A), normal (N) and wet spells (W). The black dotted line is the 1:1 line between modelled and observed data.

The difference in mean annual GPP for both CLASSIC$_{SOX}$ and CLASSIC compared to mean annual NEE-derived GPP during peak summer might be due to uncertainties associated with CLASSIC$_{SOX}$ and CLASSIC parameters (Section 2.1, 2.3). Comparing the simulated GPP against NEE-derived GPP observations across all sites shows improved GPP for CLASSIC$_{SOX}$, i.e., improved R^2, RMSE, and bias compared to CLASSIC (Fig. S4a). This finding is mainly due to the high g_c of CLASSIC$_{SOX}$ at low Ψ_s compared to CLASSIC (Fig. S3e). The underestimation of GPP at US-BZS and US-Uaf might be due to the WD parameter because we assumed the WD of the Alaskan boreal forest sites is similar to that of the Canadian boreal forest sites. Both CLASSIC$_{SOX}$ and CLASSIC underestimated GPP at US-BZS and US-Uaf, indicating probably a structural limitation of CLASSIC. The underestimation of GPP might be linked with higher observations (which itself derived from NEE, i.e., modelled), as the mean annual GPP unexpectedly increases from 5 to 8 g C m^{-2} d^{-1} from a nearby site experiencing similar environmental conditions (US-Prr, Fig. 3f-h). Moreover, the mean annual GPP from US-BZS and US-Uaf is even higher than the CA-Obs, CA-Man, and CA-Qfo sites, characterized by dense tree cover, higher AI, and MAT than US-BZS and US-Uaf (Fig. 3, Table S1). There might be uncertainties related to the WD parameter in SOX (Section 4.2) along with the issue of other hydraulic compartments of the soil-plant-atmosphere continuum being important during drought (e.g., the soil-root hydraulic conductance might decline very fast during drought; Carminati & Javaux, 2020). Higher g_s at low Ψ_s might be due to the structural limitation of SOX because SOX assumes $\Psi_r \approx \Psi_s$ and excludes the decline of soil-root hydraulic conductance during drought conditions (Eller et al., 2018; Carminati & Javaux, 2020). While CLASSIC$_{SOX}$ demonstrably improved GPP compared to CLASSIC using an SMS function, CLASSIC$_{SOX}$ simulated poorer water fluxes with an underestimated peak summer ET at CA-Obs and CA-Man (Fig. 4, S6). The underestimated ET can be attributed to the CLASSIC's evaporation scheme being effectively 'tuned' for the SMS transpiration behaviour. As transpiration changes under the SOX representation, CLASSIC's canopy and ground evaporation scheme likely needs to be reassessed. The poorer ET impacted the GPP-ET relationship with a lower R^2 for CLASSIC$_{SOX}$ (Fig. 5). The slope between GPP and ET slightly increased due to the higher GPP for CLASSIC$_{SOX}$ compared to CLASSIC (Fig. 5).

The CLASSIC$_{SOX}$ relationship between g_c and Ψ_s indicates that during low soil water potential (i.e., drought conditions), CLASSIC$_{SOX}$ simulated higher g_c because it used plant hydraulic traits instead of the SMS function used in CLASSIC (Fig. S3). Moreover, higher g_s for SOX during drought conditions is depicted in g_s response curves (Fig. 2i), where the g_s becomes approximately zero for the SMS function when the Ψ_s reaches the wilting point. While SOX simulated higher g_s even at very low Ψ_s of -5.0 MPa, and low wood density (WD = 0.18 g cm^{-3}, with Ψ_{50} = -1.59 MPa and a = 2.32, Fig. 2i). At higher VPD, the plants with higher WD keep their stomates open longer meaning their simulated g_s is higher for SOX compared to CLASSIC (Fig. 2g). All of the results for CLASSIC$_{SOX}$ better simulate stomatal conductance response under drought conditions using plant hydraulics which was underestimated with the SMS function in CLASSIC (Fig. 2, S3).

4.1 CLASSIC$_{SOX}$ limitations

In this study, we tested an implementation of SOX in CLASSIC at eight boreal forest flux tower sites. Implementing an explicit plant hydraulics parameterization in the boreal biome adds challenges to the model simulations. One of the main challenges is obtaining plant functional type/species-specific parameters (i.e. Ψ_{50} and $k_{sl,max}$) for vegetation in the boreal biome, as they are missing from the available plant hydraulic trait databases (Lin et al., 2015; Mencuccini, Rosas, et al., 2019; Choat et al., 2012; Manzoni, Vico, Porporato, & Katul, 2013). To address this challenge, we obtained WD data from NFI for the entire Canadian boreal forest and used empirical equations from Christoffersen et al. (2016) to calculate Ψ_{50} and $k_{sl,max}$ for each study site. Using WD to calculate val-

ues for plant hydraulic parameters, rather than the observed values, adds uncertainty to parameter values. Further uncertainties are due to mapping parameter values from species to PFTs, differences within the same species due to edaphic, climatic, or phenotypical factors, and measurement uncertainties. In addition, we used the SOX parameter values for shrubs, sedges, and C3 grasses from Eller et al. (2020).
CLASSIC$_{SOX}$ is significantly computationally more expensive than CLASSIC due to a higher number of optimizations required to determine the c_i. The lack of an efficient optimization algorithm (e.g. feedback control to stomatal optimization) should be addressed in future studies to ensure the model is computationally efficient enough for high-resolution large domain studies (Jones et al., 2022).

5 Conclusions

We implemented a plant hydraulics parameterization, SOX, in CLASSIC and tested the resulting CLASSIC$_{SOX}$ at the eight boreal forest flux tower sites in North America. Our study used wood density and plant hydraulic traits data, which connects the soil, plant, and atmosphere continuum in a single compartment. An explicit connection of soil and atmosphere through plants was previously missing in the existing empirically-based soil moisture stress function of CLASSIC that was used to limit photosynthesis. The plant hydraulics parameterization also proved to be more parameter parsimonious than the soil moisture stress function used in CLASSIC, reducing the number of parameters from four to one in CLASSIC$_{SOX}$. Experimental results for GPP at all sites were more consistent with the NEE-derived observations, especially under drought conditions with low soil water potential and high vapour pressure deficit. Annual accumulated GPP using the plant hydraulics parameterization (CLASSIC$_{SOX}$) at all eight sites (65 site-years) improved by 15 % compared to CLASSIC when evaluated against the NEE-derived observed GPP. While CLASSIC$_{SOX}$ improved simulated GPP under all moisture conditions (i.e. drought and non-drought), it further underestimated ET than the original CLASSIC, likely due to the evaporation scheme of CLASSIC being tailored to the existing soil moisture stress function-based transpiration scheme. Further research is needed to investigate SOX across the boreal biome and its impact upon historical and future carbon fluxes.

6 Open Research

The current version of model is available from the project website: `https://gitlab.com/cccma/classic` under the Open Government License – Canada and the GNU General Public License version 2. The version of the model (CLASSIC v.1.4) used in this study.
The model benchmarking dataset used in this study is available on Zenodo: `https://doi.org/10.5281/zenodo.7266010` (Qu, Roy, Melton, Black, et al., 2023).

Acknowledgments
This work is part of the project "Using satellite L-band observations to incorporate plant hydraulic functioning into a terrestrial ecosystem model to project future boreal forest response to drought conditions and heat stress" funded through the Canadian Space Agency (CSA) Grant 21SUESUSLB awarded to Oliver Sonnentag.

References

Anderegg, W. R., Trugman, A. T., Bowling, D. R., Salvucci, G., & Tuttle, S. E. (2019). Plant functional traits and climate influence drought intensification and land–atmosphere feedbacks. *Proceedings of the National Academy of Sciences*, *116*(28), 14071–14076.

Anderegg, W. R., & Venturas, M. D. (2020). Plant hydraulics play a critical role in earth system fluxes. *New Phytologist*, *226*(6), 1535–1538.

Best, M. J., Pryor, M., Clark, D., Rooney, G. G., Essery, R., Ménard, C., ... others (2011). The joint uk land environment simulator (jules), model description–part 1: energy and water fluxes. *Geoscientific Model Development*, *4*(3), 677–699.

Bonan, G., Williams, M., Fisher, R., & Oleson, K. (2014). Modeling stomatal conductance in the earth system: linking leaf water-use efficiency and water transport along the soil–plant–atmosphere continuum. *Geoscientific Model Development*, *7*(5), 2193–2222.

Brodribb, T. J., & Jordan, G. J. (2008). Internal coordination between hydraulics and stomatal control in leaves. *Plant, Cell & Environment*, *31*(11), 1557–1564.

Buckley, T. N. (2017). Modeling stomatal conductance. *Plant physiology*, *174*(2), 572–582.

Buckley, T. N. (2019). How do stomata respond to water status? *New Phytologist*, *224*(1), 21–36.

Carminati, A., & Javaux, M. (2020). Soil rather than xylem vulnerability controls stomatal response to drought. *Trends in Plant Science*, *25*(9), 868–880.

Choat, B., Jansen, S., Brodribb, T. J., Cochard, H., Delzon, S., Bhaskar, R., ... others (2012). Global convergence in the vulnerability of forests to drought. *Nature*, *491*(7426), 752–755.

Christoffersen, B. O., Gloor, M., Fauset, S., Fyllas, N. M., Galbraith, D. R., Baker, T. R., ... others (2016). Linking hydraulic traits to tropical forest function in a size-structured and trait-driven model (tfs v. 1-hydro). *Geoscientific Model Development*, *9*(11), 4227–4255.

Clark, D., Mercado, L., Sitch, S., Jones, C., Gedney, N., Best, M., ... others (2011). The joint uk land environment simulator (jules), model description–part 2: carbon fluxes and vegetation dynamics. *Geoscientific Model Development*, *4*(3), 701–722.

Collatz, G. J., Ball, J. T., Grivet, C., & Berry, J. A. (1991). Physiological and environmental regulation of stomatal conductance, photosynthesis and transpiration: a model that includes a laminar boundary layer. *Agricultural and Forest meteorology*, *54*(2-4), 107–136.

Collatz, G. J., Ribas-Carbo, M., & Berry, J. A. (1992). Coupled photosynthesis-stomatal conductance model for leaves of c4 plants. *Functional Plant Biology*, *19*(5), 519–538.

Cowan, I., & Farquhar, G. (1977). Stomatal function in relation to leaf metabolism and environment. *Symposia of the Society for Experimental Biology*(31), 471-505.

Cox, P., Betts, R., Bunton, C., Essery, R., Rowntree, P., & Smith, J. (1999). The impact of new land surface physics on the gcm simulation of climate and climate sensitivity. *Climate Dynamics*, *15*, 183–203.

Cox, P., Huntingford, C., & Harding, R. (1998). A canopy conductance and photosynthesis model for use in a gcm land surface scheme. *Journal of Hydrology*, *212*, 79–94.

Dewar, R. C. (2010). Maximum entropy production and plant optimization theories. *Philosophical Transactions of the Royal Society B: Biological Sciences*, *365*(1545), 1429–1435.

Dewar, R. C., Franklin, O., Mäkelä, A., McMurtrie, R. E., & Valentine, H. T. (2009). Optimal function explains forest responses to global change. *Bioscience*, *59*(2), 127–139.

Eller, C. B., Rowland, L., Mencuccini, M., Rosas, T., Williams, K., Harper, A., ... others (2020). Stomatal optimization based on xylem hydraulics (sox) improves land surface model simulation of vegetation responses to climate. *New*

Phytologist, *226*(6), 1622–1637.

Eller, C. B., Rowland, L., Oliveira, R. S., Bittencourt, P. R., Barros, F. V., Da Costa, A. C., ... others (2018). Modelling tropical forest responses to drought and el niño with a stomatal optimization model based on xylem hydraulics. *Philosophical Transactions of the Royal Society B: Biological Sciences*, *373*(1760), 20170315.

Ethier, G., Livingston, N., Harrison, D., Black, T., & Moran, J. (2006). Low stomatal and internal conductance to co2 versus rubisco deactivation as determinants of the photosynthetic decline of ageing evergreen leaves. *Plant, Cell & Environment*, *29*(12), 2168–2184.

Farquhar, G., Schulze, E. D., & Kuppers, M. (1980). Responses to humidity by stomata of nicotiana glauca l. and corylus avellana l. are consistent with the optimization of carbon dioxide uptake with respect to water loss. *Functional Plant Biology*, *7*(3), 315–327.

Ficklin, D. L., & Novick, K. A. (2017). Historic and projected changes in vapor pressure deficit suggest a continental-scale drying of the united states atmosphere. *Journal of Geophysical Research: Atmospheres*, *122*(4), 2061–2079.

Field, C. B., Jackson, R. B., & Mooney, H. A. (1995). Stomatal responses to increased co2: implications from the plant to the global scale. *Plant, Cell & Environment*, *18*(10), 1214–1225.

Franklin, O., Harrison, S. P., Dewar, R., Farrior, C. E., Brännström, Å., Dieckmann, U., ... others (2020). Organizing principles for vegetation dynamics. *Nature plants*, *6*(5), 444–453.

Friend, A. (1995). Pgen: an integrated model of leaf photosynthesis, transpiration, and conductance. *Ecological Modelling*, *77*(2-3), 233–255.

Grantz, D. (1990). Plant response to atmospheric humidity. *Plant, Cell & Environment*, *13*(7), 667–679.

Green, J., Zhang, Y., Luo, X., & Keenan, T. (2024). Systematic underestimation of canopy conductance sensitivity to drought by earth system models. *AGU Advances*, *5*(1), e2023AV001026.

He, X., Wada, Y., Wanders, N., & Sheffield, J. (2017). Intensification of hydrological drought in california by human water management. *Geophysical Research Letters*, *44*(4), 1777–1785.

Hickler, T., Prentice, I. C., Smith, B., Sykes, M. T., & Zaehle, S. (2006). Implementing plant hydraulic architecture within the lpj dynamic global vegetation model. *Global Ecology and Biogeography*, *15*(6), 567–577.

Jacobs, C. M. J. (1994). *Direct impact of atmospheric co 2 enrichment on regional transpiration*. Wageningen University and Research.

Jones, S., Eller, C. B., & Cox, P. M. (2022). Application of feedback control to stomatal optimisation in a global land surface model. *Frontiers in Environmental Science*, *10*, 2167.

Kennedy, D., Swenson, S., Oleson, K. W., Lawrence, D. M., Fisher, R., Lola da Costa, A. C., & Gentine, P. (2019). Implementing plant hydraulics in the community land model, version 5. *Journal of Advances in Modeling Earth Systems*, *11*(2), 485–513.

Kyker-Snowman, E., Lombardozzi, D. L., Bonan, G. B., Cheng, S. J., Dukes, J. S., Frey, S. D., ... others (2022). *Increasing the spatial and temporal impact of ecological research: A roadmap for integrating a novel terrestrial process into an earth system model*. Wiley Online Library.

Lambert, M. S., Tang, H., Aas, K. S., Stordal, F., Fisher, R. A., Fang, Y., ... Parmentier, F.-J. W. (2022). Inclusion of a cold hardening scheme to represent frost tolerance is essential to model realistic plant hydraulics in the arctic–boreal zone in clm5. 0-fates-hydro. *Geoscientific Model Development*, *15*(23), 8809–8829.

Leuning, R. (1995). A critical appraisal of a combined stomatal-photosynthesis

model for c3 plants. *Plant, Cell & Environment*, *18*(4), 339–355.

Lin, Y.-S., Medlyn, B. E., Duursma, R. A., Prentice, I. C., Wang, H., Baig, S., ... others (2015). Optimal stomatal behaviour around the world. *Nature Climate Change*, *5*(5), 459–464.

Manzoni, S., Vico, G., Katul, G., Palmroth, S., Jackson, R. B., & Porporato, A. (2013). Hydraulic limits on maximum plant transpiration and the emergence of the safety–efficiency trade-off. *New Phytologist*, *198*(1), 169–178.

Manzoni, S., Vico, G., Porporato, A., & Katul, G. (2013). Biological constraints on water transport in the soil–plant–atmosphere system. *Advances in Water Resources*, *51*, 292–304.

Martínez-Vilalta, J., Poyatos, R., Aguadé, D., Retana, J., & Mencuccini, M. (2014). A new look at water transport regulation in plants. *New phytologist*, *204*(1), 105–115.

Martin-StPaul, N., Delzon, S., & Cochard, H. (2017). Plant resistance to drought depends on timely stomatal closure. *Ecology letters*, *20*(11), 1437–1447.

Medlyn, B. E., Barton, C., Broadmeadow, M., Ceulemans, R., De Angelis, P., Forstreuter, M., ... others (2001). Stomatal conductance of forest species after long-term exposure to elevated co2 concentration: a synthesis. *New Phytologist*, *149*(2), 247–264.

Medlyn, B. E., De Kauwe, M. G., Zaehle, S., Walker, A. P., Duursma, R. A., Luus, K., ... others (2016). Using models to guide field experiments: A priori predictions for the co 2 response of a nutrient-and water-limited native eucalypt woodland. *Global Change Biology*, *22*(8), 2834–2851.

Medlyn, B. E., Duursma, R. A., Eamus, D., Ellsworth, D. S., Prentice, I. C., Barton, C. V., ... Wingate, L. (2011). Reconciling the optimal and empirical approaches to modelling stomatal conductance. *Global Change Biology*, *17*(6), 2134–2144.

Melton, J. R., & Arora, V. (2016). Competition between plant functional types in the canadian terrestrial ecosystem model (ctem) v. 2.0. *Geoscientific Model Development*, *9*(1), 323–361.

Melton, J. R., Arora, V. K., Wisernig-Cojoc, E., Seiler, C., Fortier, M., Chan, E., & Teckentrup, L. (2020). Classic v1. 0: the open-source community successor to the canadian land surface scheme (class) and the canadian terrestrial ecosystem model (ctem)–part 1: Model framework and site-level performance. *Geoscientific Model Development*, *13*(6), 2825–2850.

Mencuccini, M., Manzoni, S., & Christoffersen, B. (2019). Modelling water fluxes in plants: from tissues to biosphere. *New Phytologist*, *222*(3), 1207–1222.

Mencuccini, M., Rosas, T., Rowland, L., Choat, B., Cornelissen, H., Jansen, S., ... others (2019). Leaf economics and plant hydraulics drive leaf: wood area ratios. *New Phytologist*, *224*(4), 1544–1556.

Miralles, D. G., Gentine, P., Seneviratne, S. I., & Teuling, A. J. (2019). Land–atmospheric feedbacks during droughts and heatwaves: state of the science and current challenges. *Annals of the New York Academy of Sciences*, *1436*(1), 19–35.

Mott, K. A. (1988). Do stomata respond to co2 concentrations other than intercellular? *Plant physiology*, *86*(1), 200–203.

NFI. (accessed 08 25, 2022). National forest inventory. 2021. canada's national forest inventory –ground-plot data, version 2.0. [dataset]. *NFI*.

Palmer, W. C. (1965). *Meteorological drought* (Vol. 30). US Department of Commerce, Weather Bureau.

Paschalis, A., De Kauwe, M. G., Sabot, M., & Fatichi, S. (2024). When do plant hydraulics matter in terrestrial biosphere modelling? *Global Change Biology*, *30*(1), e17022.

Prentice, I. C., Dong, N., Gleason, S. M., Maire, V., & Wright, I. J. (2014). Balancing the costs of carbon gain and water transport: testing a new theoretical

framework for plant functional ecology. *Ecology letters*, *17*(1), 82–91.

Qu, B., Roy, A., Melton, J. R., Baltzer, J. L., Ryu, Y., Detto, M., & Sonnentag, O. (2023). Optimizing maximum carboxylation rate for north america's boreal forests in the canadian land surface scheme including biogeochemical cycles (classic) v. 1.3. *EGUsphere*, *2023*, 1–19.

Qu, B., Roy, A., Melton, J. R., Black, T. A., Amiro, B., Euskirchen, E. S., ... others (2023). A boreal forest model benchmarking dataset for north america: a case study with the canadian land surface scheme including biogeochemical cycles (classic) [dataset]. *Environmental Research Letters*, *18*(8), 085002.

Rahmstorf, S., & Coumou, D. (2011). Increase of extreme events in a warming world. *Proceedings of the National Academy of Sciences*, *108*(44), 17905–17909.

Ronda, R., De Bruin, H., & Holtslag, A. (2001). Representation of the canopy conductance in modeling the surface energy budget for low vegetation. *Journal of Applied Meteorology and Climatology*, *40*(8), 1431–1444.

Sabot, M. E., De Kauwe, M. G., Pitman, A. J., Medlyn, B. E., Ellsworth, D. S., Martin-StPaul, N. K., ... others (2022). One stomatal model to rule them all? toward improved representation of carbon and water exchange in global models. *Journal of Advances in Modeling Earth Systems*, *14*(4), e2021MS002761.

Sabot, M. E., De Kauwe, M. G., Pitman, A. J., Medlyn, B. E., Verhoef, A., Ukkola, A. M., & Abramowitz, G. (2020). Plant profit maximization improves predictions of european forest responses to drought. *New Phytologist*, *226*(6), 1638–1655.

Savage, V. M., Bentley, L. P., Enquist, B. J., Sperry, J. S., Smith, D., Reich, P. B., & Von Allmen, E. (2010). Hydraulic trade-offs and space filling enable better predictions of vascular structure and function in plants. *Proceedings of the National Academy of Sciences*, *107*(52), 22722–22727.

Seager, R., Hooks, A., Williams, A. P., Cook, B., Nakamura, J., & Henderson, N. (2015). Climatology, variability, and trends in the us vapor pressure deficit, an important fire-related meteorological quantity. *Journal of Applied Meteorology and Climatology*, *54*(6), 1121–1141.

Seiler, C., Melton, J. R., Arora, V. K., & Wang, L. (2021). Classic v1. 0: the open-source community successor to the canadian land surface scheme (class) and the canadian terrestrial ecosystem model (ctem)–part 2: Global benchmarking [software]. *Geoscientific Model Development*, *14*(5), 2371–2417.

Sellers, P. J., Tucker, C. J., Collatz, G. J., Los, S. O., Justice, C. O., Dazlich, D. A., & Randall, D. A. (1996). A revised land surface parameterization (sib2) for atmospheric gcms. part ii: The generation of global fields of terrestrial biophysical parameters from satellite data. *Journal of climate*, *9*(4), 706–737.

Sperry, J. S., Adler, F., Campbell, G., & Comstock, J. (1998). Limitation of plant water use by rhizosphere and xylem conductance: results from a model. *Plant, Cell & Environment*, *21*(4), 347–359.

Sperry, J. S., & Tyree, M. T. (1988). Mechanism of water stress-induced xylem embolism. *Plant physiology*, *88*(3), 581–587.

Sperry, J. S., Venturas, M. D., Anderegg, W. R., Mencuccini, M., Mackay, D. S., Wang, Y., & Love, D. M. (2017). Predicting stomatal responses to the environment from the optimization of photosynthetic gain and hydraulic cost. *Plant, cell & environment*, *40*(6), 816–830.

Trugman, A., Medvigy, D., Mankin, J., & Anderegg, W. (2018). Soil moisture stress as a major driver of carbon cycle uncertainty. *Geophysical Research Letters*, *45*(13), 6495–6503.

Tyree, M. T., Davis, S. D., & Cochard, H. (1994). Biophysical perspectives of xylem evolution: is there a tradeoff of hydraulic efficiency for vulnerability to dysfunction? *IAWA journal*, *15*(4), 335–360.

Tyree, M. T., & Sperry, J. S. (1989). Vulnerability of xylem to cavitation and em-

bolism. *Annual review of plant biology*, *40*(1), 19–36.

Ukkola, A., De Kauwe, M., Pitman, A., Best, M., Abramowitz, G., Haverd, V., ... Haughton, N. (2016). Land surface models systematically overestimate the intensity, duration and magnitude of seasonal-scale evaporative droughts. *Environmental Research Letters*, *11*(10), 104012.

Wang, Y., Sperry, J. S., Anderegg, W. R., Venturas, M. D., & Trugman, A. T. (2020). A theoretical and empirical assessment of stomatal optimization modeling. *New Phytologist*, *227*(2), 311–325.

Wang, Y., Sperry, J. S., Venturas, M. D., Trugman, A. T., Love, D. M., & Anderegg, W. R. (2019). The stomatal response to rising co2 concentration and drought is predicted by a hydraulic trait-based optimization model. *Tree physiology*, *39*(8), 1416–1427.

Wells, N., Goddard, S., & Hayes, M. J. (2004). A self-calibrating palmer drought severity index. *Journal of climate*, *17*(12), 2335–2351.

Williams, M., Law, B. E., Anthoni, P. M., & Unsworth, M. H. (2001). Use of a simulation model and ecosystem flux data to examine carbon–water interactions in ponderosa pine. *Tree physiology*, *21*(5), 287–298.

Williams, M., Rastetter, E., Fernandes, D., Goulden, M., Wofsy, S., Shaver, G., ... Nadelhoffer, K. (1996). Modelling the soil-plant-atmosphere continuum in a quercus–acer stand at harvard forest: the regulation of stomatal conductance by light, nitrogen and soil/plant hydraulic properties. *Plant, Cell & Environment*, *19*(8), 911–927.

Zomer, R. J., Xu, J., & Trabucco, A. (2022). Version 3 of the global aridity index and potential evapotranspiration database. *Scientific Data*, *9*(1), 409.